Asian Journal of Chemistry; Vol. 34, No. 2 (2022), 331-341

ASIAN JOURNAL OF CHEMISTRY

https://doi.org/10.14233/ajchem.2022.23483

Photocatalytic Degradation of Rhodamine B and Malachite Green by Cobalt Sulfide Nanoparticles

GUNJAN CHAUHAN[1,*] and MANJEET SHARMA[2]

[1]Department of Chemistry, Maharishi Markandeshwar (Deemed to be University), Mullana-133207, India
[2]Department of Chemistry, Himachal Pradesh University, Shimla-171005, India

*Corresponding author: E-mail: gunjan.chauhan@mmumullana.org

Received: 17 August 2021; *Accepted*: 22 October 2021; *Published online*: 11 January 2022; AJC-20656

Present study reports the simple and cost effective thermolytic method for the synthesis of cobalt sulphide nanoparticles (CoS NPs). The PXRD spectrum of cobalt sulphide (CdS) nanoparticles exhibited four peaks indexed to (100), (101), (102) and (110) crystal planes. The average particle size observed from DLS and PXRD was in the range 4.81-12.20 nm. A blue shift in band gap was observed from UV-visible spectra. The FESEM and TEM studies revealed that cobalt sulfide nanoparticles are of cubic and rectangle shapes. FTIR spectra of hexadecylamine (HDA) capped CoS NPs exhibited ν(N-H) absorption around 3350-3240 cm^{-1}. The stretching frequency due to ν(Co-S) appeared in the region 334-332 cm^{-1}. Proton NMR (^1H) spectra of CoS NPs showed signals at nearly same positions as in case of capping agent, suggesting its capping nature. ESI-MS analyses of cobalt sulphide nanoparticles displayed peak at m/z = 124.93 corresponding to the $[CoS_2]^+$ ion. Thermogravimetric curves showed single step decomposition corresponding to 84.28% weight loss and 15.72% as final residue due to cobalt oxide. The degradation rate of rhodamine B and malachite green dyes after irradiating with sunlight showed 92-94% degradation while irradiated with UV-light of 4.8 eV show much slower degradation rate.

Keywords: Cobalt sulphide nanoparticles, Thermolytic method, Rhodamine B, Malachite Green, Photocatalytic degradation.

INTRODUCTION

The global energy crisis and environmental pollution due to rapid industrialization have become two of the greatest challenges of human society in the 21st century [1-3]. The growing rate of industrialization increases emission of effluents from different industries, which poses serious threats to several living forms due to their adverse effects. Toxic water-pollutants and pollution associated with hazardous wastes containing organic dyes are major pollutants in wastewaters released from textile and other industries. Due to higher stability of modern synthetic dyes with high concentration of organics in the effluents, conventional treatment methods are ineffective for the degradation and complete colour removal [4,5]. In order to reduce the negative effects of dye contaminated wastewater to humans and the environment, it must be treated carefully before discharge into main streams.

Photocatalytic degradation has emerged as cost-effective, economical and one of the most promising technology because of its ability to utilize solar energy directly (at ground level the energy of ultraviolet light only constitutes for a small fraction of sunlight @ ~4%), while the visible light constitutes for a large fraction of sunlight (~ 45%), which suggests the feasibility of using solar energy as the best solution to these critical problems [6-8] for producing solar fuels, alleviating the environmental pollution [9-11] and sowing to its ability to convert these into safer end products such as CO_2, H_2O [12]. Therefore, much efforts has been devoted toward converting solar energy into an applicable energy medium through various technologies.

Photocatalysis is a process by which a semiconductor material absorbs light of energy more than or equal to its band-gap, thereby generating electrons and holes, which can further generate free radicals in the system to oxidize the substrate. The resulting free radicals are very efficient oxidizers of organic matter [13,14]. The photoconversion efficiency of the photocatalytic reactions is still low and they are far from practical application, because of the rapid electron-hole recombination and poor light utilization of semiconductors [15-17]. Therefore, developing of low-cost and robust photocatalyst with significantly improved photocatalytic activity remains challenging task for the researchers.

At present, semiconductor materials have been studied extensively in advanced oxidation processes as photocatalysts due to their peculiar and fascinating physico-chemical properties [18]. Nano-scale semiconductor particles allow greater photon adsorption on the photocatalyst surface [19,20] as they have higher surface area to volume ratio than their bulk counter parts and thus recombination of the electron-hole pair within the semiconductor particle is drastically reduced as particle size decreases. Metal sulfide semiconductor materials are widely used in different field of applications such as solar energy absorption [21], high electrical conductivity [22,23] and chemical sensing capabilities. Cobalt sulfides, a significant class of semiconductors (CoS, Co_3S_4 and Co_9S_8) are widely used in a wide range of applications including dye sensitized solar cells, electrochemical devices and in photocatalysis [24-28]. Veerabhadram *et al.* [29] have reported the solvothermal synthesis of CuS nanoparticles with particle size < 20 nm and 34.37 m^2/g specific surface area. The cadmium sulphide (CdS) nanoparticles capped in the xanthan gum acted as an efficient photocatalyst for dye degradation under sunlight than artificial visible and UV lights. Soltani *et al.* [30] have reported the study of the variation in composition of ZnS and CdS nanoparticles with degradation efficiency of about 73% after 6 h irradiation time and were found to be efficient for degradation of methylene blue. The photocatalytic activities of TiO_2 have been studied by many researchers and show photocatalytic behaviour of TiO_2 under UV light [31-34], which limits its practical applications. Since few years photocatalytic activities have been carried out for various dyes by doping, co-doping of metals, inorganic elements in TiO_2 [35-38] and composites of TiO_2 [39,40], using visible light.

The aim of the present investigation was to prepare cobalt sulphide (CoS) nanoparticles through thermolysis method by reacting stoichiometric amounts of precursors {[Co(4-MPipzcdtH)$_2$]$(CH_3COO)_2$ and [Co(MorphcdtH)$_2$]$(CH_3COO)_2$} with hexadecylamine, which acted as capping agent to prevent agglomeration of the nanosized particles. The CoS nanoparticles have been characterized using various techniques. Further their potential for the dyes degradation has also been investigated against rhodamine B and malachite green.

EXPERIMENTAL

All the solvents and chemicals *viz*. ethanol, methanol, dimethyl sulphoxide, toluene, carbon disulphide, 1-methylpiperazine, morpholine, hexadecylamine, triphenylphosphine, cobalt acetate tetrahydrate, rhodamine B dye and malachite green dye were received from Merck and used as received.

Synthesis of ligands: The morpholinecarbodithioic acid (MorphcdtH) and 4-methylpiperazine-1-carbodithioic acid (4-MPipzcdtH) were synthesized by insertion of CS_2 into the N–H bond of heterocyclic amines, morpholine and 1-methylpiperazine using literature methods [41].

Synthesis of precursors [*bis*(4-methylpiperazine-1-carbodithioicacid)cobalt(II)acetate] {[Co(4-MPipzcdtH)$_2$]$(CH_3COO)_2$}, [*bis*(4-morphpiperazine-1-carbodithioic acid)cobalt(II) acetate {[Co(MorphcdtH)$_2$]$(CH_3COO)_2$}: To a continuously stirred methanolic solution of $Co(CH_3COO)_2 \cdot 4H_2O$ (0.100 g; 0.401 mmol) was added the ultrasonicated methanolic solution of ligands [4-MPipzcdtH (0.141 g; 0.799 mmol), 4-morphcdtH (0.130 g; 0.799 mmol)] in slightly less than stoichiometric amount. Stirring was continued for another 3 h. The green precipitates of precursors [Co(4-MPipzcdtH)$_2$]$(CH_3COO)_2$ and [Co(MorphcdtH)$_2$]$(CH_3COO)_2$ formed were washed with methanol 4-5 times (eqns. 1 and 2). These were collected by centrifugation technique and dried overnight by keeping in $CaCl_2$ desiccator.

$$Co(CH_3COO)_2 \cdot 4H_2O + 2(4\text{-MPipzcdtH}) \longrightarrow [Co(4\text{-MPipzcdtH})_2](CH_3COO)_2 \quad (1)$$

$$Co(CH_3COO)_2 \cdot 4H_2O + 2(\text{MorphcdtH}) \longrightarrow [Co(\text{MorphcdtH})_2](CH_3COO)_2 \quad (2)$$

[Co(4-MPipzcdtH)$_2$]$(CH_3COO)_2$: Green, yield: 99%. Decomposition temperature: 230 ºC. m.f.: $C_{16}H_{30}N_4S_4O_4Co$; *m.w.* 528.93. CHN analysis calcd. (found) %: C, 36.29 (35.10); H, 5.67 (5.29); N, 10.58 (10.13); S, 24.19 (23.99); O, 12.09 (12.01); Co, 11.14 (11.04).

[Co(MorphcdtH)$_2$]$(CH_3COO)_2$: Green, yield: 99%. Decomposition temperature: 210 ºC. m.f.: $C_{14}H_{24}O_6N_2S_4Co$; *m.w.* 502.93). CHN analysis calcd. (found) %: C, 33.40 (33.31); H, 4.77 (4.52); N, 5.56 (5.22); S, 25.45 (25.10); O, 19.08 (18.90); Co, 11.71 (11.20).

Synthesis of hexadecylamine capped CoS nanoparticles by thermolysis method: The synthesis of CoS nanoparticles capped by hexadecylamine (HDA) (1.37 g; 5.7 mmol) has been carried out using precursors {[Co(MorphcdtH)$_2$]$(CH_3COO)_2$ (0.100 g; 1.99 mmol)} and {[Co(4-MPipzcdtH)$_2$]$(CH_3COO)_2$, (0.105 g; 1.99 mmol)}, which were dispersed in triphenylphosphine (TPP) by thoroughly grinding in a pestle mortar. The mixture was dissolved in hot HDA in a silica crucible and placed at 185 ºC in muffle furnace (for 1 h). It was cooled to room temperature. Black solid mass was taken out of furnace. Aliquots of sample were stirred in methanol for 10-15 min in order to dissolve excess of HDA and the medium TPP. The grey colour precipitates were separated by centrifugation while supernatant was decanted off. The precipitates were further dispersed in toluene and washed 4-5 times using centrifugation technique to get pure form of CoS nanoparticles and dried in a $CaCl_2$ desiccator. The CoS·2HDA nanoparticles were soluble in DMSO on sonication and partially soluble in other solvents. The HDA capped CoS nanoparticles were obtained according to eqns. 3 and 4:

$$[Co(4\text{-MPipzcdtH})_2](CH_3COO)_2 + 3HDA \xrightarrow{185\ ^oC} CoS{\cdot}2HDA + HDA \quad (3)$$

$$[Co(\text{MorphcdtH})_2](CH_3COO)_2 + 3HDA \xrightarrow{185\ ^oC} CoS{\cdot}2HDA + HDA \quad (4)$$

Yield: 95%, decomposition temperature (using [Co(MorphcdtH)$_2$]$(CH_3COO)_2$: 270 ºC and using [Co(4-MPipzcdtH)$_2$]$(CH_3COO)_2$: 290 ºC.

Detection method: Particle size (average diameter) of HDA capped CoS nanoparticles was measured using Modular Dynamic Light Scatter System (Nanotrac wave model MN401,

λ = 780 nm, from microtrac) in a range of 0.8 to 6500 nm in 30 s. X-ray diffraction (XRD) pattern of the nanoparticles in powder form was obtained on a diffractometer system [XPERT–PRO] in 2θ range of 10º-80º with a step size of 0.050 having 1 s counting time at each step using Cu*K*α (λ = 1.540 Å) radiation source. Surface Plasmon resonance spectrum of CoS nanoparticles in solvent methanol as reference was recorded on Bio-chem UV-visible spectrophotometer (range 900-200 nm). Thermal analysis (TG/DSC) was carried out on TGA Model 2950 and DSC-Model 2920, Make-TA Instruments, USA using thermocouple Pt/Pt-Rh (10%) with a temperature range of 20-1200 ºC. Analysis was carried out at a heating rate of 10 ºC min^{-1} in a Pt crucible under static air atmosphere with Al_2O_3 as reference. The instrument was periodically calibrated with $CuSO_4 \cdot 5H_2O$. WATERS, Q-TOF MICROMASS (ESI-MS) spectrometer (mass range: 80-2200 *m/z*) was used for recording mass spectra of nanoparticles. Sample solution was prepared in DMSO: (2.0 mg/10.0 mL) and introduced into electron spray ionization (ESI) source by MS injection. The mass spectrometer is coupled with Waters 2795 HPLC having quaternary pumping configured for flow rates from 0.05-5.0 mL/min attached to auto sampler configured with a 100 µL syringe. Field emission scanning electron microscopy (FE-SEM) measurements on powder/dispersion in methanol of nanoparticles were performed on Hitachi ultra high resolution scanning electron microscope SU8010 connected to EDS element quantification system. The instrument has resolution of 1.0 nm (point to point) with 1-15 kV operating voltage. TEM measurements of as synthesized sample of nanoparticles dispersed in methanol were made by fixing them on a copper-supported carbon film on a Hitachi microscope (H-7500) equipped with CCD camera. The instrument has resolution of 0.36 (0.4) nm (point to point) with 40-120 kV operating voltage. FTIR spectra of nanoparticles were recorded as KBr pellets on Nicolet 5700 FT infrared spectrophotometer in the 4000-600 cm^{-1} region. While FTIR spectra were recorded as nujol mull with cesium chloride plates as windows in the 600-200 cm^{-1} region. ^1H NMR spectra of deuterated DMSO/cyclohexane solution of nanoparticles were recorded on BRUKER AVANCE II 400 NMR spectrophotometer using TMS as an internal standard. For dye degradation study 50 mL 10^{-4} M (aq.) solution of dye was treated with 50 mg of HDA capped cobalt sulfide and placed in sunlight. Percentage degradation was checked by taking small aliquots of reaction mixture at definite time intervals and absorbance was noted on Biochem UV-visible spectrophotometer (range 900-200 nm).

RESULTS AND DISCUSSION

The synthesized CoS·2HDA nanoparticles synthesized from precursors, *viz.* $[Co(MorphcdtH)_2](CH_3COO)_2$ and $[Co(4\text{-}MPipzdtH)_2](CH_3COO)_2$ were characterized by using various techniques. The particle size measured in methanolic solution (sonicated for 15 min) of CoS nanoparticles Fig. 1(a-b) was found to be 4.81 nm and 11.73 nm for $[Co(MorphcdtH)_2](CH_3COO)_2$ and $[Co(4\text{-}MPipzcdtH)_2](CH_3COO)_2$, respectively.

The PXRD patterns of HDA capped CoS nanoparticles synthesized from precursors, *viz.* $[Co(MorphcdtH)_2](CH_3COO)_2$ and $[Co(4\text{-}MPipzdtH)_2](CH_3COO)_2$ showed broad diffraction peaks at 2θ values lying in range: (a) 28.36º-29.91º, (b) 36.10º-37.97º (Fig. 2a-b), which have been indexed to (100), (101), (102) and (110) crystal planes of hexagonal CoS, respectively [42,43]. Average crystallite size of the CoS nanoparticles was determined by using the Debye-Scherrer equation: $Dp = k\lambda/\beta_{1/2} \cos\theta$ [44], where diffraction pattern (Dp) represents particle size in nm, k is shape factor (usually taken as 0.94), λ is the wavelength of X-ray (1.54 Å for Cu*K*α), $\beta_{1/2}$ is the full width at half maximum (FWHM) of peak and θ is Bragg's angle in radians. The calculated crystallite size from four planes was found to be in the range of 7.8-12.2 nm for CoS·2HDA obtained from precursors $[Co(MorphcdtH)_2](CH_3COO)_2$ and $[Co(4\text{-}MPipzcdtH)_2](CH_3COO)_2$. The 2θ values and their respective d-spacing values well matched with those of standard JCPDS card no. 65-3418 for cobalt sulphide with hexagonal structure [42,43]. No new phases were observed.

Effect of nature of capping agent *i.e.* HDA on crystal structure has further been studied by calculating lattice constants '*a*' and '*c*'. The lattice constants 'a' and 'c' lies in range 3.371-3.377 and 5.11-5.15, respectively. The data is given in Tables 1 and 2, which is comparable to that of literature [45].

UV-visible studies: The UV-visible spectra of HDA capped CoS·2HDA nanoparticles obtained using precursors, $[Co(MorphcdtH)_2](CH_3COO)_2$ and $[Co(4\text{-}MPipzcdtH)_2](CH_3COO)_2$

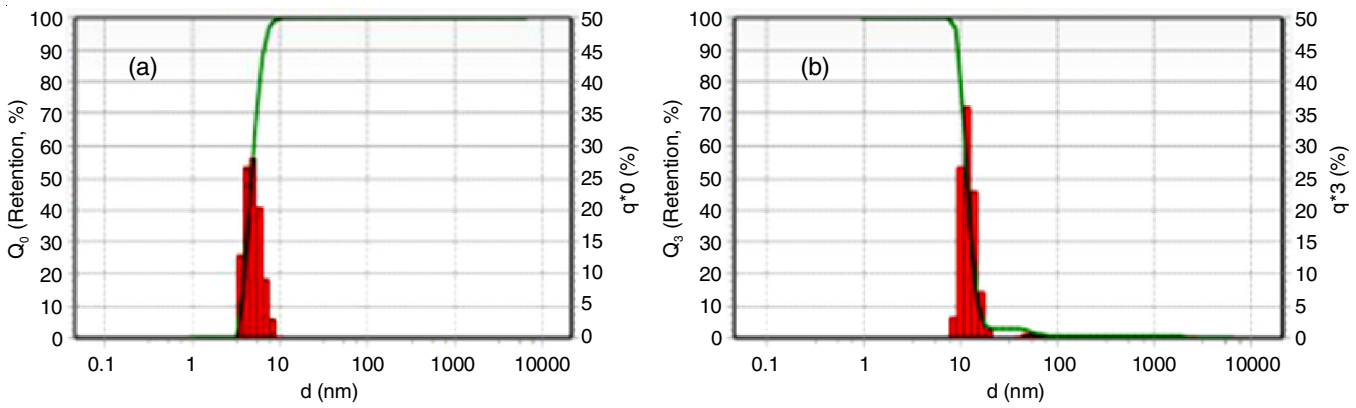

Fig. 1. Particle size distribution of CoS·2HDA nanoparticles prepared from precursors (a) $[Co(MorphcdtH)_2](CH_3COO)_2$ and (b) $[Co(4\text{-}MPipzcdtH)_2](CH_3COO)_2$

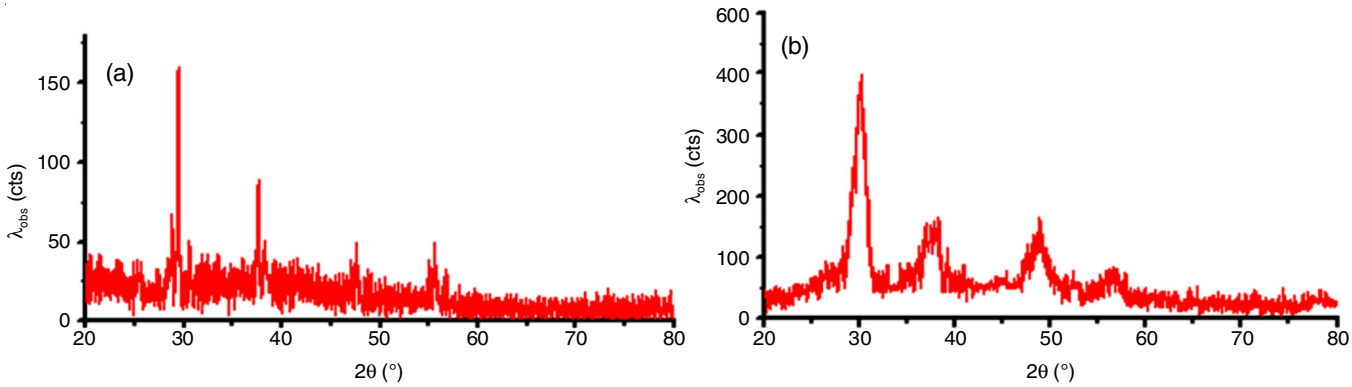

Fig. 2. PXRD patterns of CoS·2HDA nanoparticles prepared from precursors (a) $[Co(MorphcdtH)_2](CH_3COO)_2$ and (b) $[Co(4\text{-}MPipzdtH)_2]\text{-}(CH_3COO)_2$

TABLE-1
PXRD DATA OF CoS·2HDA NANOPARTICLES PREPARED FROM PRECURSOR $[Co(MorphcdtH)_2](CH_3COO)_2$

2θ (°)	d-Spacing (Å)	FWHM (°)	Dp (nm)	Lattice constant	
				(a)	(c)
29.73	2.9245	1.0637	8.1	3.377	5.15
37.87	2.5407	1.1247	7.8	3.375	5.14
47.60	1.9255	1.0935	8.3	3.374	5.12
55.25	1.6855	1.1426	8.2	3.371	5.11

TABLE-2
PXRD DATA OF CoS·2HDA NANOPARTICLES PREPARED FROM PRECURSOR $[Co(4\text{-}MPipzcdtH)_2](CH_3COO)_2$

2θ (°)	d-Spacing (Å)	FWHM (°)	Dp (nm)	Lattice constant	
				(a)	(c)
28.36	2.9237	0.7317	11.7	3.376	5.15
37.25	2.5419	0.7689	11.3	3.375	5.15
47.99	1.9276	0.7701	11.8	3.374	5.13
56.87	1.6865	0.7740	12.2	3.373	5.14

exhibited an absorption peak at 230 and 235 nm, respectively as shown in Fig. 3(a-b) which is blue shifted from that of bulk CoS (1127.27 nm, band gap 1.01 eV) [46]. This shift could be associated with the tuning of band gap for absorption in the visible region. The existence of peak around 230-260 nm have been regarded as excitation peak for CoS and is indicative of the existence of CoS as nanoparticles [46]. The fundamental absorption, which corresponds to excitation of electron from valance band to conduction band, can be used to determine the optical band gap of the synthesized CoS nanoparticles by using Tauc relationship [47] $(\varepsilon h\nu) = C\ (h\nu - E_g)^n$ where C = constant, ε is molar extinction coefficient, E_g is average band gap of material and n depends upon type of transition. The band gaps of CoS·2HDA nanoparticles prepared from precursors $[Co(MorphcdtH)_2](CH_3COO)_2$, $[Co(4\text{-}MPipzcdtH)_2](CH_3COO)_2$ have been evaluated to be 5.39 and 5.28 eV, respectively. These values are greater than that for bulk CoS having a band gap of 1.01 eV. Increase in the band gap energies of CoS·2HDA nanoparticles is due to the quantum confinement effect resulting from decrease in size of particles. Slight variation in positions and broadness of peaks from bulk to capped CoS nanoparticles can be attributed to absorptions of capping agents in the same range.

Thermal studies: The thermal stability and decomposition behaviour of CoS·2HDA from precursors, $[Co(MorphcdtH)_2]\text{-}(CH_3COO)_2$ and $[Co(4\text{-}MPipzcdtH)_2](CH_3COO)_2$ were studied

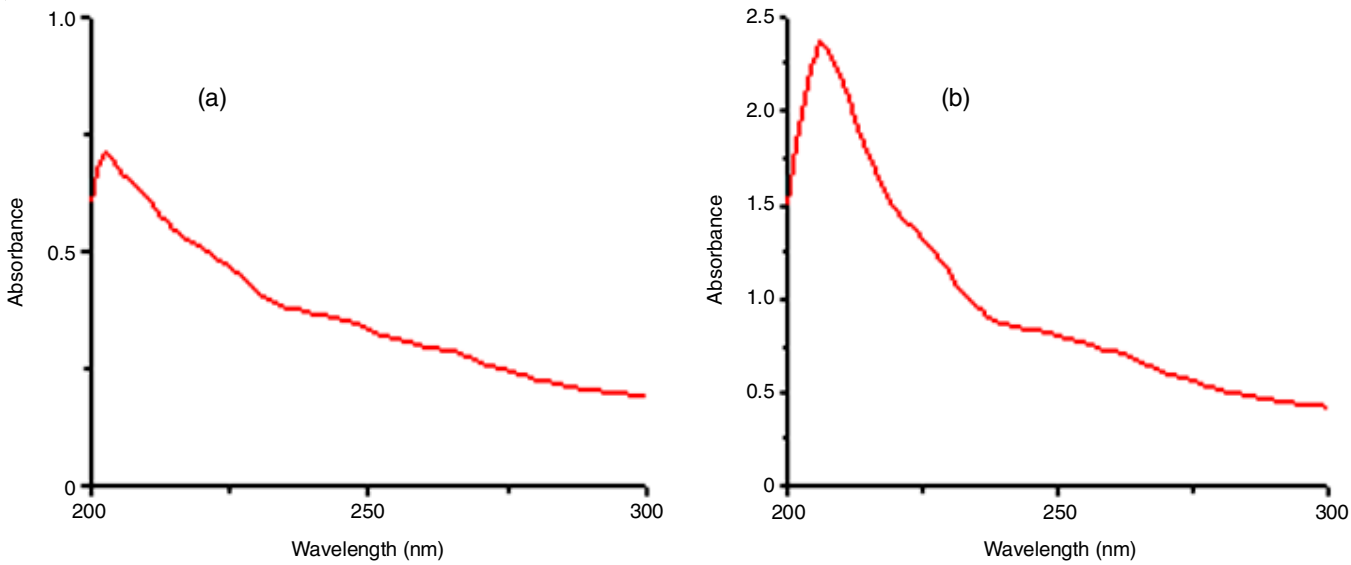

Fig. 3. Electronic absorption spectrum of CoS·2HDA nanoparticles prepared from precursors (a) $[Co(MorphcdtH)_2](CH_3COO)_2$ and (b) $[Co(4\text{-}MPipzcdtH)_2](CH_3COO)_2$

in a controlled manner under oxygen atmosphere to explore the thermal behaviour of complexes using TG and DSC analysis and to check the nature and composition of thermolytic end products formed. Different constituents of particular group vary with composition and structure of complex which can be easily determined using thermal studies. Hexadecylamine (HDA) capped CoS nanoparticles exhibited single step decomposition in temperature range 280-310 ºC. Sharp exotherms were observed in DSC patterns between 300-330 ºC for HDA capped CoS nanoparticles.

The CoS·2HDA nanoparticles synthesized from the precursors $[Co(MorphcdtH)_2](CH_3COO)_2$ and $[Co(4\text{-}MPipzdtH)_2](CH_3COO)_2$ showed their initial decomposition temperature (IDT) at 280 and 290 ºC exhibiting single step decomposition (Fig. 4). Thermogram of CoS·2HDA nanoparticles prepared from precursor $[Co(4\text{-}MPipzcdtH)_2](CH_3COO)_2$ with plateau in the curve showed IDT at 290 ºC having single step decomposition with mass loss of 84.28 % in temperature range of 290-400 ºC. The mass loss for the CoS·2HDA nanoparticles prepared from precursors, *viz.* $[Co(Morp\text{-}hcdtH)_2](CH_3COO)_2$ and $[Co(4\text{-}MPipzdtH)_2](CH_3COO)_2$ corresponds to two moles of HDA and yielding as CoO final product of decomposition (Table-3). The DSC curve of CoS· 2HDA nanoparticles obtained from precursor $[Co(4\text{-}MPipzcdtH)_2](CH_3COO)_2$ exhibited a sharp exotherm at 330 ºC. A perusal of the TG/DSC curves of CoS·2HDA nanoparticles prepared from the precursors $[Co(MorphcdtH)_2](CH_3COO)_2$ and $[Co(4\text{-}MPipzcdtH)_2](CH_3COO)_2$ was indicative of the IDT, decomposition range and exotherms at 280, 300 ºC; 290, 330 ºC, respectively. The CoO as end product in all the cases remained stable for further increase in temperature up to 800 ºC. The nature of end products was further complimented by recording the PXRD of residues.

Powder XRD studies: The powder X-ray diffraction of the residues of TG study of CoS·2HDA nanoparticles prepared from precursors $[Co(MorphcdtH)_2](CH_3COO)_2$ and $[Co(4\text{-}MPipzcdtH)_2](CH_3COO)_2$ (Fig. 5) were carried out to find out the composition of final product. The PXRD pattern of residues of all the complexes showed peaks at 2θ values of 37.89º, 42.55º, 61.27º, 73.19º and 75.32° corresponding to crystal planes 111, 200, 220, 311 and 222 rock-salt structure of CoO (JCPDS card no. 431004) [48]. No diffraction peaks of Co_3O_4 or metallic Co were observed.

TABLE-3
THERMAL DECOMPOSITION DATA OF CoS NPs

	Nanoparticles (m.w.)	
	CoS·2HDA {precursor: $[Co(MorphcdtH)_2](CH_3COO)_2$} 573.85	CoS·2HDA {precursor: $[Co(4\text{-}MPipzcdtH)_2](CH_3COO)_2$} 573.85
Sample mass (mg)	1.89	2.43
IDT (°C)	280	290
Stage	1st	1st
TG temp. (°C)	270-420	280-420
Mass loss % (Exp/Theo)	84.20/84.28 (482.95/482.92)	84.17/84.28 (482.98/482.92)
Mass left % (Exp/Theo)	15.8/15.72 (90.90/90.93)	15.83/15.72 (90.87/90.93)
Species lost	2HDA	2HDA
Species formed	CoO + O	CoO + O
DSC nature (Exo/Endo)	300	330

FESEM-EDAX studies: In present study, the FESEM and EDAX of the synthesized CoS·2HDA nanoparticles synthesized from the precursors, $[Co(MorphcdtH)_2](CH_3COO)_2$ and $[Co(4\text{-}MPipzcdtH)_2](CH_3COO)_2$ have been carried out. Fig. 6 showed the FE-SEM images and EDAX spectra of the CoS·2HDA nanoparticles obtained from $[Co(MorphcdtH)_2](CH_3COO)_2$ and $[Co(4\text{-}MPipzcdtH)_2](CH_3COO)_2$, respectively. The EDAX spectrum of CoS·2HDA nanoparticles prepared from $[Co(4\text{-}MPipzcdtH)_2](CH_3COO)_2$ revealed 50.48 wt.% of cobalt, 42.40 wt.% of sulphur, 1.81 wt.% of nitrogen and 5.25 wt.% of carbon. The CoS·2HDA nanoparticles prepared from $[Co(MorphcdtH)_2](CH_3COO)_2$ revealed 52.2 wt.% of cobalt, 39.23 wt.% of sulphur, 1.42 wt.% of nitrogen and 5.75 wt.% of carbon. FESEM images of HDA capped CoS nanoparticles exhibit the cubic and rectangle shapes. However, the actual size cannot be determined by FESEM due to the resolution limitations of the instrument. The EDAX spectrum of HDA capped nanoparticles confirmed the elemental composition.

TEM studies: In present study, the TEM micrographs of CoS·2HDA nanoparticles synthesized from precursors, *viz.*

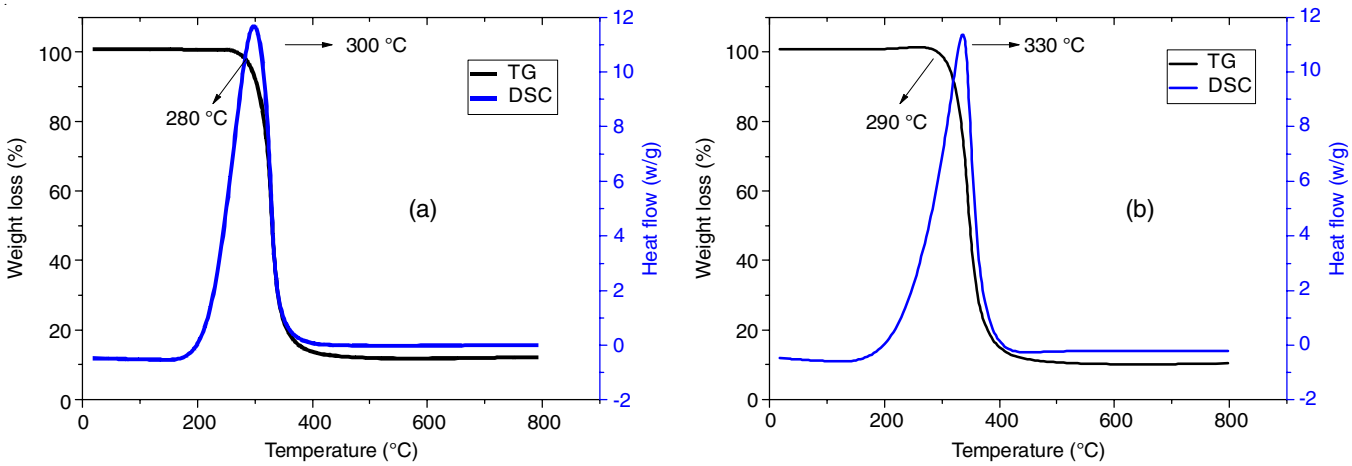

Fig. 4. TG/DSC curves of CoS·2HDA NPs prepared from precursors (a) $[Co(MorphcdtH)_2](CH_3COO)_2$ and (b) $[Co(4\text{-}MPipzcdtH)_2](CH_3COO)_2$

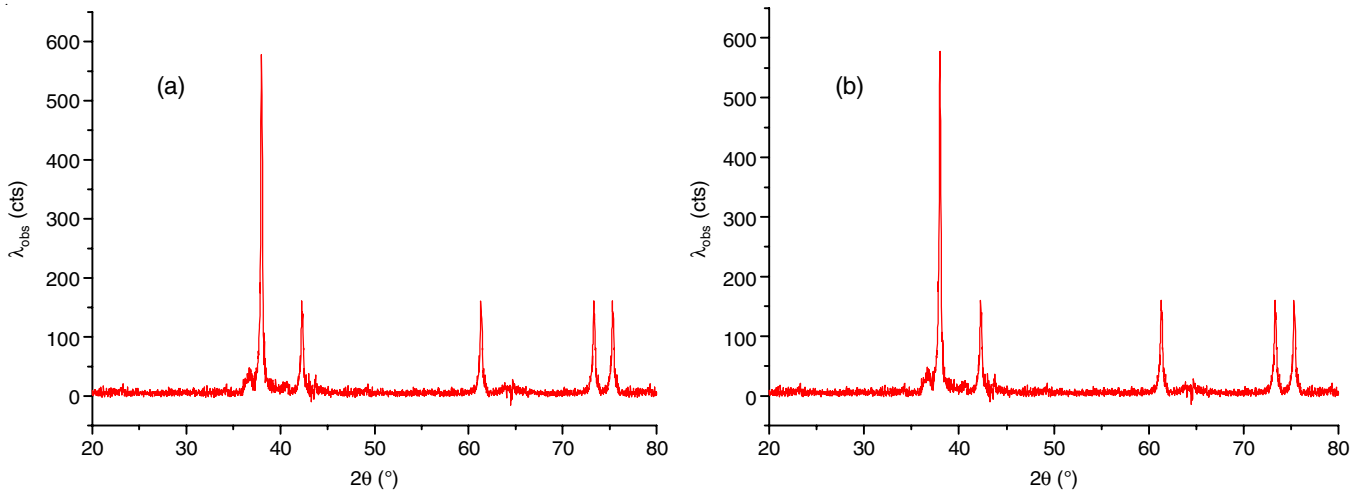

Fig. 5. PXRD of TG residue of Cos·2HDA nanoparticles prepared from precursors (a) $[Co(MorphcdtH)_2](CH_3COO)_2$ and (b) $[Co(4\text{-}MPipzcdtH)_2](CH_3COO)_2$

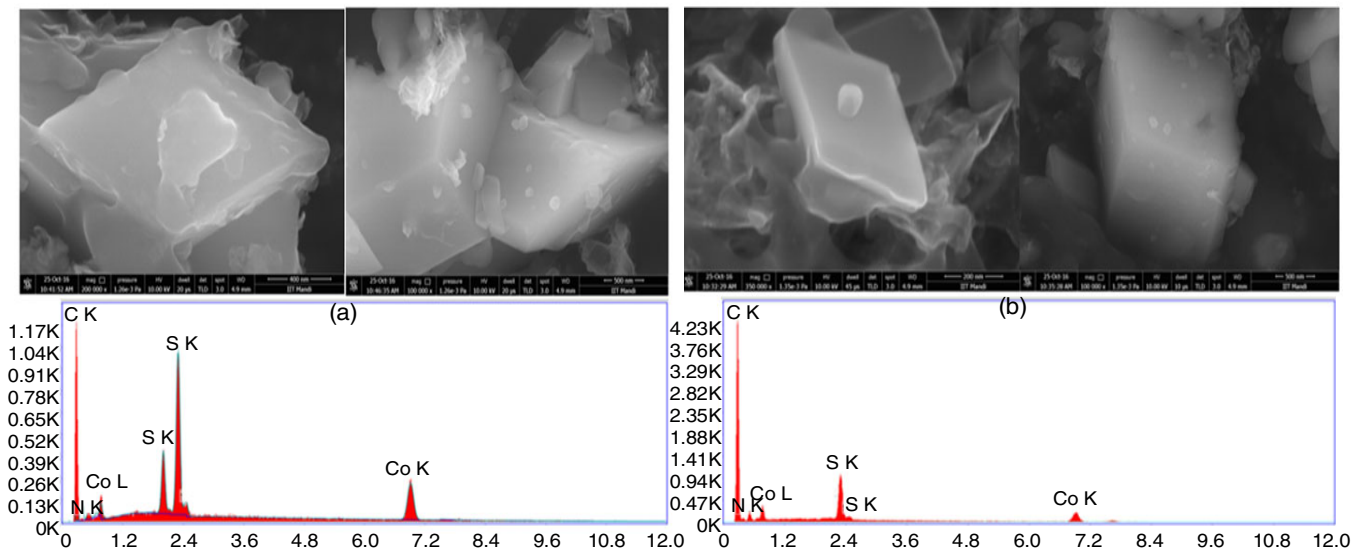

Fig. 6. FESEM images and EDAX spectrum of CoS·2HDA nanoparticles prepared from precursors (a) $[Co(MorphcdtH)_2](CH_3COO)_2$ and (b) $[Co(4\text{-}MPipzcdtH)_2](CH_3COO)_2$

$[Co(MorphcdtH)_2](CH_3COO)_2$ and $[Co(4\text{-}MPipzdtH)_2]\text{-}(CH_3COO)_2$ were recorded. Typical TEM micrographs (Fig. 7) of CoS nanoparticles capped by HDA exhibited the rect-angle shape. The average particle size falling in the range 5-20 nm in diameter follow the increasing order as CoS· 2HDA nanoparticles (precursor: $Co(MorphcdtH)_2](CH_3COO)_2$ < CoS·2HDA nanoparticles (precursor: $[Co(4\text{-}MPipzcdtH)_2](CH_3COO)_2$. Critical examination of average particle size of CoS nanoparticles capped from HDA inferred that core diameter increases with increase in length of carbon chain at fourth position in heterocyclic ring of carbodithioic acid. These observations are in consonance with the trend observed in DLS study. TEM micrographs further indicated that smaller particles apparently agglomerated to form larger non-spherical particles, most plausibly due to some overlapped lattice effects of capping agent, which is used in greater stoichiometric amount than required. The observation in terms of morphology is consistent with FESEM study.

^{1}H NMR studies: Under present investigation ^{1}H NMR spectrum of HDA capped CoS nanoparticles obtained from the $[Co(MorphcdtH)_2](CH_3COO)_2$ and $[Co(4\text{-}MPipzdtH)_2]\text{-}(CH_3COO)_2$ have been studied and compared with that of pure HDA (Fig. 8). The proton resonance signals showed by pure HDA at δ 0.88 ppm due to CH_3-, δ 1.26 ppm due to $(CH_2)14$ -, δ 2.68 ppm because of CH_2- attached to amine group and at δ 1.76 ppm due to NH_2- protons [49]. The signals around δ 3.65 ppm (NH), δ3.74-3.78 ppm (2, 3, 5 and 6-CH_2) and δ 2.96 ppm (CH_3) for 4-MPipzcdtH were absent in ^{1}H NMR spectra and thus rule out the presence of precursor molecules in synthesized CoS nanoparticles. The signals of HDA appeared at similar position as that of in CoS nanoparticles, which confirmed the existence of HDA as capping agent onto CoS nanoparticles obtained by thermolysis method.

FTIR studies: FTIR spectra of CoS·2HDA nanoparticles synthesized from the precursors by thermolysis route $[Co(MorphcdtH)_2](CH_3COO)_2$ and $[Co(4\text{-}MPipzcdtH)_2](CH_3COO)_2$

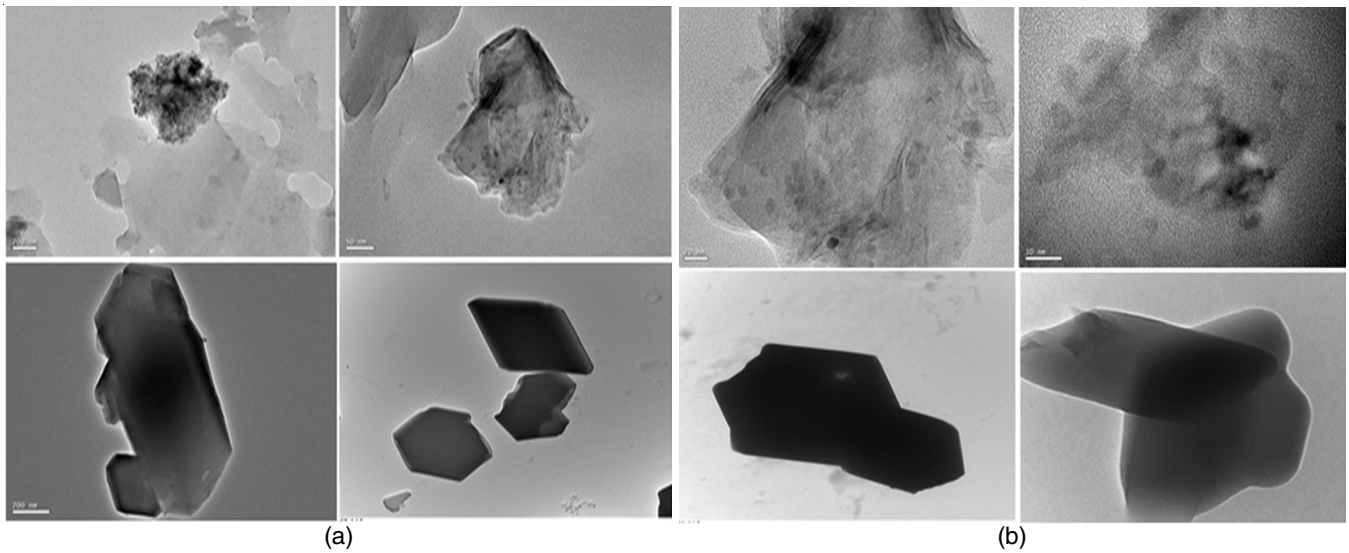

Fig. 7. TEM micrographs of CoS·2HDA nanoparticles prepared from precursors (a) $[Co(4\text{-}MPipzcdtH)_2](CH_3COO)_2$ and (b) $[Co(4\text{-}PPipzcdtH)_2](CH_3COO)_2$

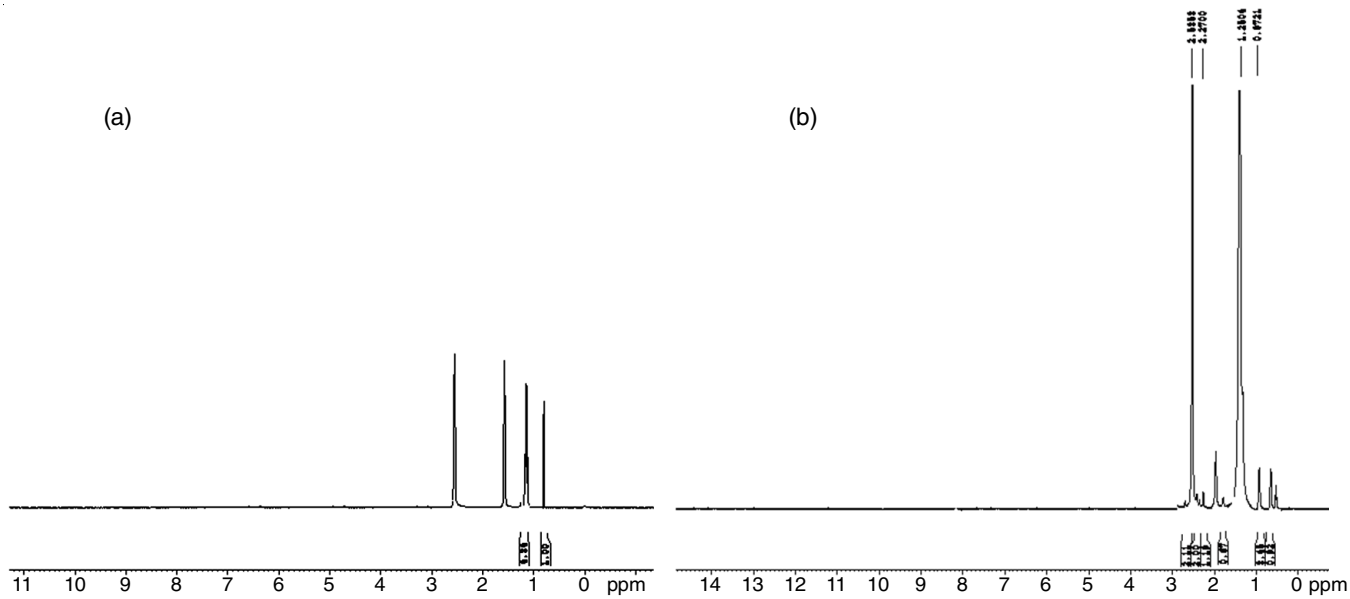

Fig. 8. ^1H NMR spectrum of CoS·2HDA nanoparticles prepared from precursors (a) $[Co(4\text{-}MPipzcdtH)_2](CH_3COO)_2$ and (b) $[Co(MorphcdtH)_2](CH_3COO)_2$

have been investigated by FTIR spectroscopy. The FTIR spectrum of hexadecylamine is characterized by the stretching frequency in the range 3358-3232 cm^{-1} due to ν(N-H) of amino group. Another region of interest is NH_2 scissoring which was observed at 1608 cm^{-1} and C-N stretching which appeared at 1112 cm^{-1}. FTIR spectrum of HDA showed two vibrational bands around 2914 and 2847 cm^{-1} due to the CH_2 antisymmetric and symmetric stretching vibrational modes, respectively. The C-H band of CH_3 group in HDA exhibited stretching vibration at 2954 cm^{-1}. The spectral band due to -CH_2 has been identified to lie at 719 cm^{-1} [46,50]. FTIR spectra of HDA capped CoS nano-particles exhibited ν(N-H) absorption around 3350-3240 cm^{-1} as shown in Fig. 9. The stretching frequencies due to N-H band appeared in range 1606-1600 cm^{-1} while that of C-N stret-ching frequencies lies in the range 1112-1107 cm^{-1}. The vibra-tional modes due to ν(C-H) of terminal CH_3 group of alkyl chain appeared in the region 2954-2960 cm^{-1} with very small shift of the order of 4-6 cm^{-1} as compared to free HDA. The stretching frequency due to ν(M-S) [46,50] appeared in the region 334-332 cm^{-1}.

ESI-MS studies: The ESI-MS analyses of HDA capped CoS nanoparticles obtained from $[Co(MorphcdtH)_2](CH_3COO)_2$ and $[Co(4\text{-}MPipzcdtH)_2](CH_3COO)_2$ has also been carried out (Fig. 10). Mass spectra of CoS·2HDA nanoparticles displayed peaks due to their molecular masses at *m/z* = 573.85 (11%) and *m/z* = 573.85 (10%), respectively. Fragmentation patterns are very similar, indicating structural resemblance of CoS nano-particles. The prominent mass ions corresponding to *m/z* = 543.85, 346.85, 149.85 and 102.85 have been identified to be $\{CoS.(NH_2(CH_2)_{14}CH_2)_2\}^+$, $\{CoS.NH_2CH_2NH_2(CH_2)_{14}\}^+$, {CoS.

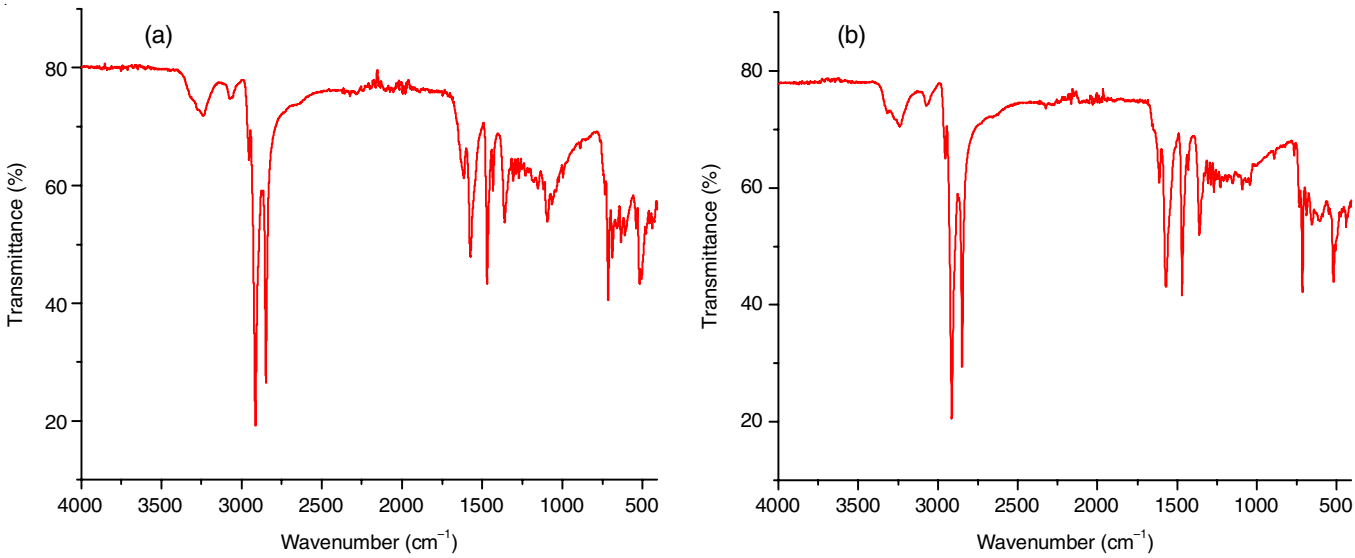

Fig. 9. FTIR spectrum of CoS·2HDA nanoparticles prepared from precursor (a) $[Co(MorphcdtH)_2](CH_3COO)_2$ and (b) $[Co(4\text{-}MPipzcdtH)_2](CH_3COO)_2$

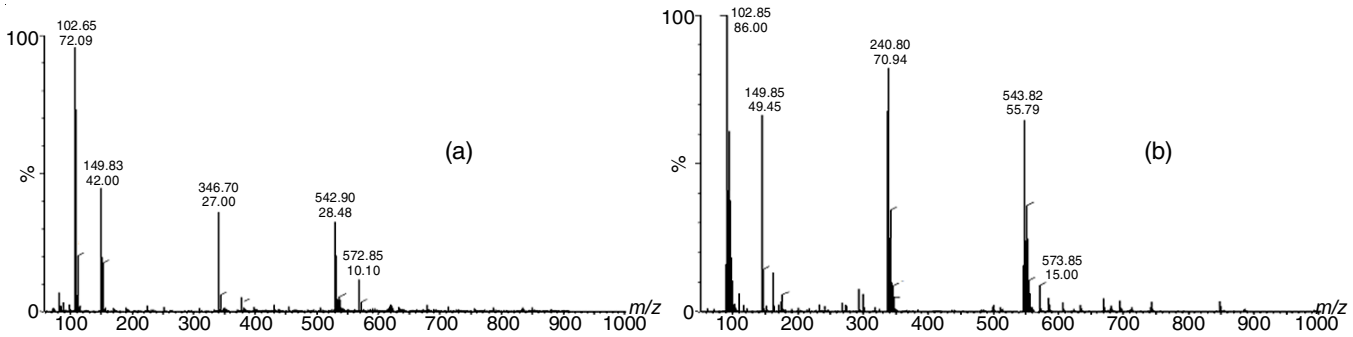

Fig. 10. Mass spectrum of CoS·2HDA nanoparticles prepared from precursors (a) $[Co(4\text{-}MPipzcdtH)_2](CH_3COO)_2$ and (b) $[Co(MorphcdtH)_2](CH_3COO)_2$

$(NH_2CH_2)_2\}^+$ and $[CoCS]^+$, respectively. The proposed fragmentation pattern of CoS·2HDA nanoparticles is shown in Fig. 11.

Photocatalytic studies: In present study, the photocatalytic behaviour of CoS nanoparticles at a concentration of 0.001-0.005 g was analyzed by studying degradation of rhodamine B and malachite green. In the experiment 50 mg of CoS·2HDA nanoparticles were added to 50 mL, 10^{-4} M (aq.) solution of each dye. The decrease of absorbance values of dye solutions at λ_{max} of dye after irradiation at definite time intervals was the rate of colour change and therefore photodegradation efficiency of nanoparticles. The degradation (D) percentage was calculated as:

$$D\ (\%) = 100 \times \frac{(A_o - A_t)}{A_o}$$

where A_o and A_t are the initial and at time t absorbance of the sample, respectively. Degradation percentage was calculated in between 90-120 min. Decrease in the wavelength with irradiation time of malachite green and rhodamine B dyes with CoS·2HDA nanoparticles are shown in Figs. 12 and 13, respectively. Effect of acidic and alkaline pH was also tested while studying dye degradation behaviour and best degradation was obtained at pH 7. The present study finds importance from the point of view that amount of the CoS·2HDA nanoparticles required for degradation as well as the total degradation time of malachite green and rhodamine B were comparable to that reported in literature [51-56].

Conclusion

The CoS nanoparticles have been synthesized by the thermolysis method, dispersed in triphenylphosphine and hexadecylamine (HDA) act as capping agent. The nanoparticles were characterized by several techniques which confirmed the purity and high density growth. The DLS and XRD analysis gave particle size between 4.81-12.2 nm. Increase in band gap from UV-visible spectrum confirmed reduction in the size of nano-particles upon capping. The CoS nanoparticles were stable up to 270 ºC as shown by thermogravimetric study and CoO remained as final residue. ESI-MS analyses of HDA capped CoS nanoparticles displayed peaks due to their molecular masses at *m/z* = 573.85. Fragmentation patterns are very similar, indicating structural resemblance of CoS nanoparticles. Almost complete photocatalytic degradation of malachite green and rhodamine B dyes was observed in the presence of sunlight when CoS nanoparticles were used as photocatalyst. The CoS nanoparticles obtained using precursors, $[Co(MorphcdtH)_2](CH_3COO)_2$ and $[Co(4\text{-}MPipzcdtH)_2](CH_3COO)_2$ have acted as highly efficient catalysts under visible light irradiation, providing a promising alternative to purify the water contaminated

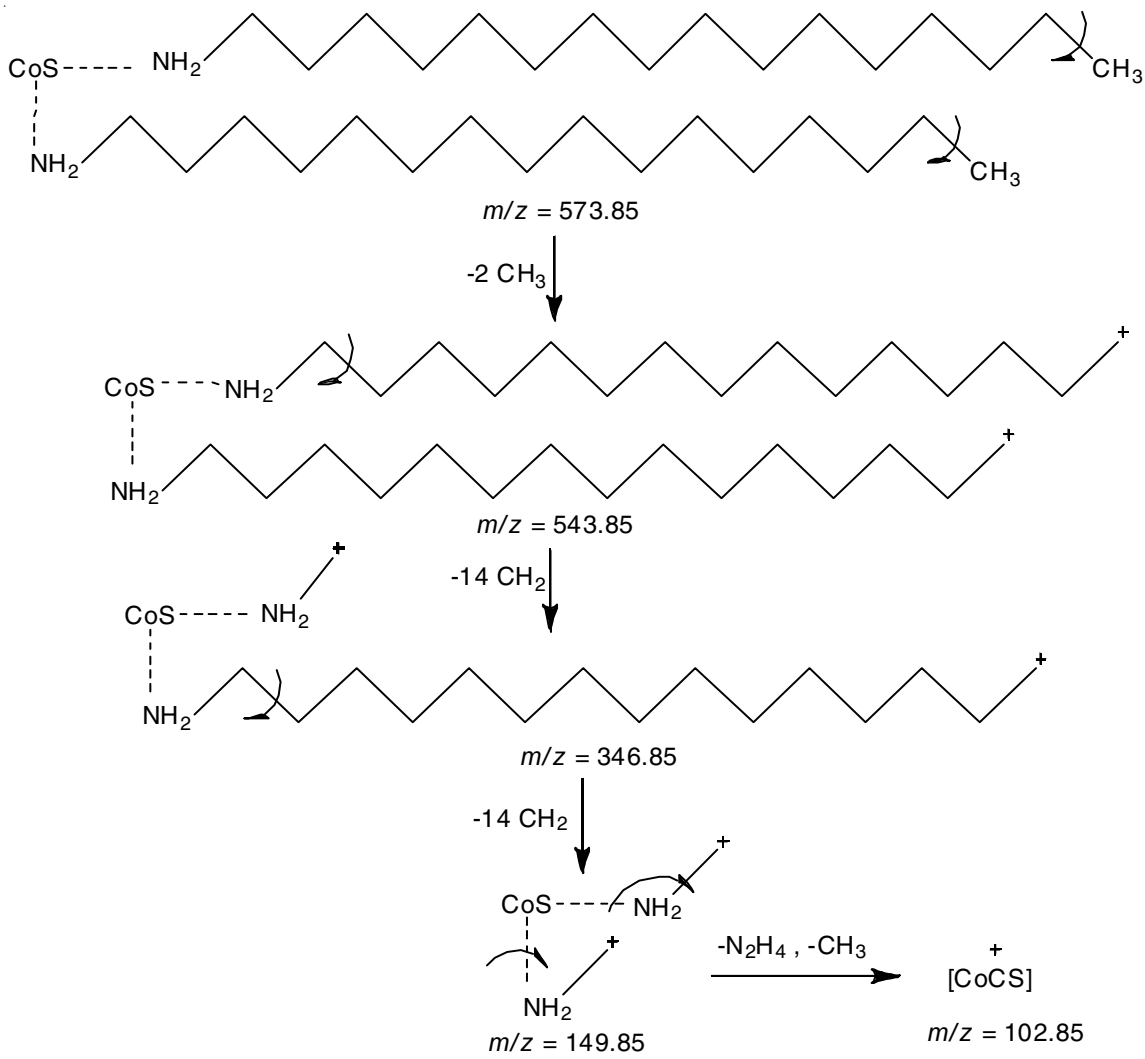

Fig. 11. Proposed fragmentation pattern of CoS·2HDA nanoparticles prepared from precursors $[Co(4\text{-}MPipzcdtH)_2](CH_3COO)_2$ and $[Co(MorphcdtH)_2](CH_3COO)_2$

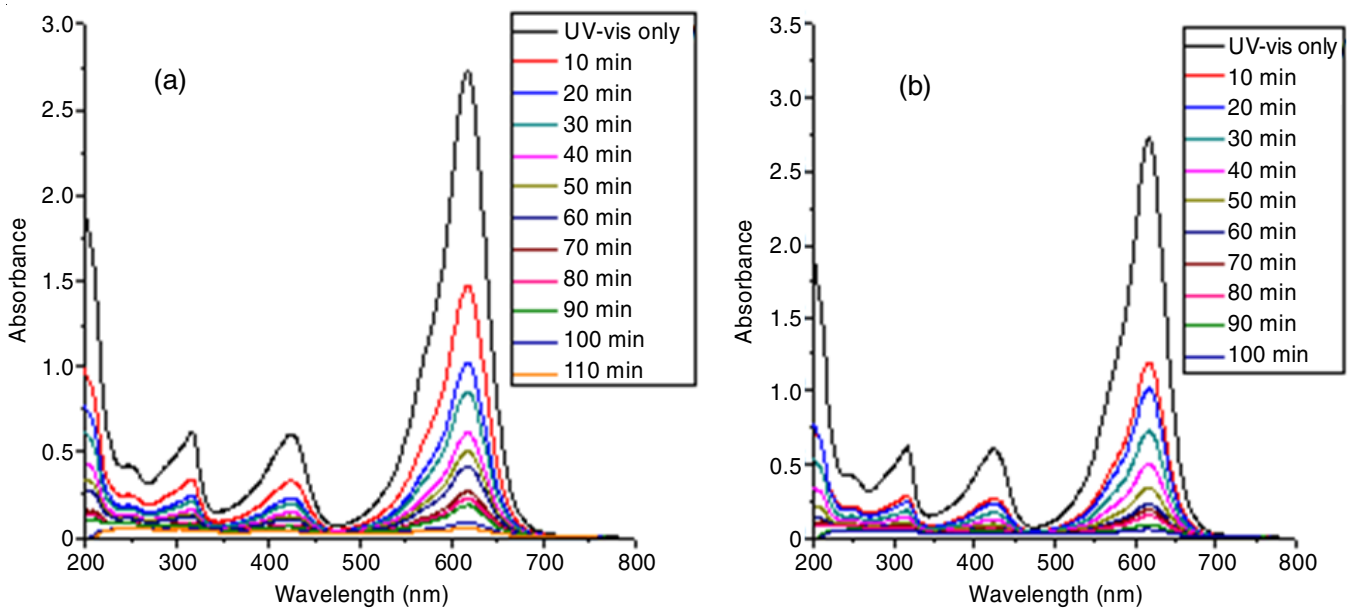

Fig. 12. Absorption spectral changes of malachite green on treatment with CoS·2HDA nanoparticles prepared from precursors (a) $[Co(MorphcdtH)_2](CH_3COO)_2$ and (b) $[Co(4\text{-}MPipzcdtH)_2](CH_3COO)_2$

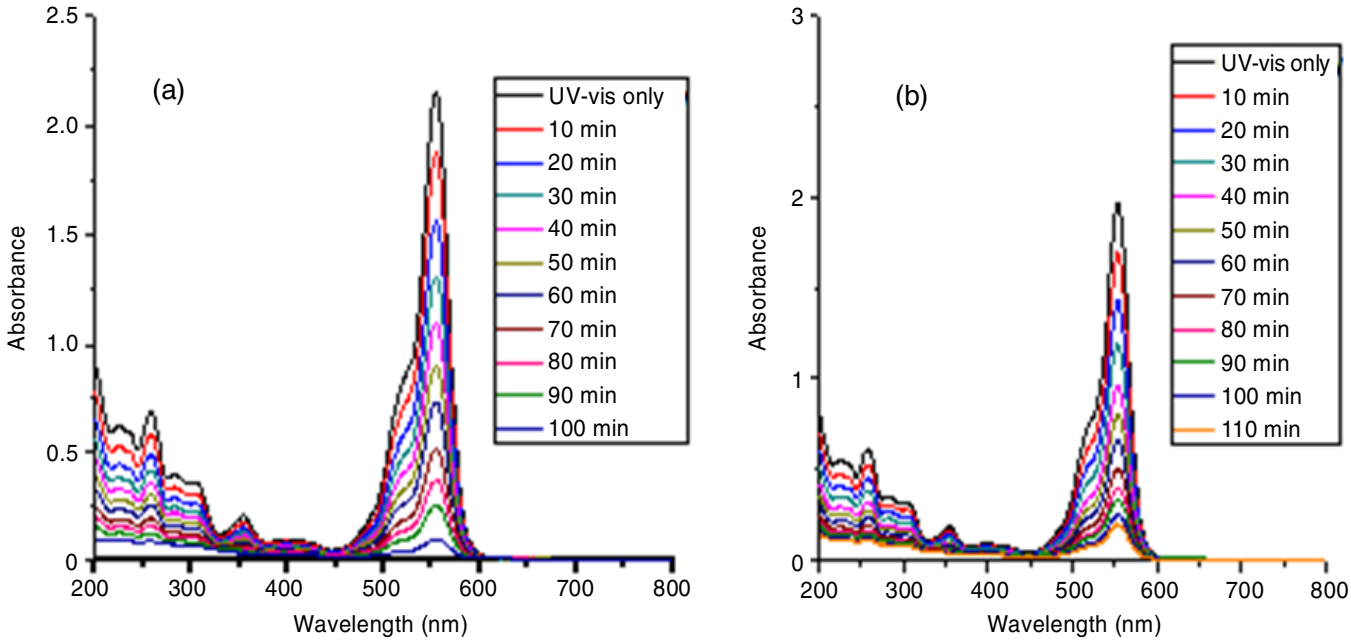

Fig. 13. Absorption spectral changes of rhodamine B dye on treatment with CoS·2HDA nanoparticles prepared from precursors (a) $[Co(MorphcdtH)_2](CH_3COO)_2$ and (b) $[Co(4\text{-}MPipzcdtH)_2](CH_3COO)_2$

with malachite green and rhodamine B dyes. All these findings provide a considerable approach to the preparation of nanoparticles and support the photocatalytic activity with enhanced efficiency.

CONFLICT OF INTEREST

The authors declare that there is no conflict of interests regarding the publication of this article.

REFERENCES

1. J. Yu, J.X. Low, W. Xiao, P. Zhou and M. Jaroniec, *J. Am. Chem. Soc.*, **136**, 8839 (2014); https://doi.org/10.1021/ja5044787
2. J. Yang, D. Wang, H. Han and C. Li, *Acc. Chem. Res.*, **46**, 1900 (2013); https://doi.org/10.1021/ar300227e
3. J.R. Ran, J. Zhang, J.G. Yu, M. Jaroniec and S.Z. Qiao, *Chem. Soc. Rev.*, **43**, 7787 (2014); https://doi.org/10.1039/C3CS60425J
4. V.K. Gupta and Suhas, *J. Environ. Manage.*, **90**, 2313 (2009); https://doi.org/10.1016/j.jenvman.2008.11.017
5. V.K. Gupta, P.J.M. Carrott, M.M.L. Ribeiro Carrott and Suhas, *Crit. Rev. Environ. Sci. Technol.*, **39**, 783 (2009); https://doi.org/10.1080/10643380801977610
6. X. Wang, W. Bi, P. Zhai, X. Wang, H. Li, G. Mailhot and W. Dong, *Appl. Surf. Sci.*, **360**, 240 (2016); https://doi.org/10.1016/j.apsusc.2015.10.229
7. Y. Sohn, W. Huang and F. Taghipour, *Appl. Surf. Sci.*, **396**, 1696 (2017); https://doi.org/10.1016/j.apsusc.2016.11.240
8. R.A. He, S.W. Cao and J.G. Yu, *Wuli Huaxue Xuebao*, **32**, 2841 (2016); https://doi.org/10.3866/PKU.WHXB201611021
9. Q. Huang, J.G. Yu, S.W. Cao, C. Cui and B. Cheng, *Appl. Surf. Sci.*, **358**, 350 (2015); https://doi.org/10.1016/j.apsusc.2015.07.082
10. J. Schneider, M. Matsuoka, M. Takeuchi, J. Zhang, Y. Horiuchi, M. Anpo and D.W. Bahnemann, *Chem. Rev.*, **114**, 9919 (2014); https://doi.org/10.1021/cr5001892
11. Z. Ni, Y. Sun, Y. Zhang and F. Dong, *Appl. Surf. Sci.*, **365**, 314 (2016); https://doi.org/10.1016/j.apsusc.2015.12.231
12. S. Kato, Y. Hirano, M. Iwata, T. Sano, K. Takeuchi and S. Matsuzawa, *J. Appl. Catal. Environ. Biol.*, **57**, 109 (2005); https://doi.org/10.1016/j.apcatb.2004.10.015
13. W. Panpa, P. Sujaridworakun and S. Jinawath, *Appl. Catal. B*, **80**, 271 (2008); https://doi.org/10.1016/j.apcatb.2007.11.029
14. C. Yogi, K. Kojima, N. Wada, H. Tokumoto, T. Takai, T. Mizoguchi and H. Tamiaki, *Thin Solid Films*, **516**, 5881 (2008); https://doi.org/10.1016/j.tsf.2007.10.050
15. J.X. Low, B. Cheng and J.G. Yu, *Appl. Surf. Sci.*, **392**, 658 (2017); https://doi.org/10.1016/j.apsusc.2016.09.093
16. S.W. Cao, J.X. Low, J.G. Yu and M. Jaroniec, *Adv. Mater.*, **27**, 2150 (2015); https://doi.org/10.1002/adma.201500033
17. W. Chen, T.Y. Liu, T. Huang, X.H. Liu, G.R. Duan, X.J. Yang and S.M. Chen, *RSC Adv.*, **5**, 101214 (2015); https://doi.org/10.1039/C5RA18302B.
18. A. Taha, *Spectrochim. Acta A Mol. Biomol. Spectrosc.*, **59**, 1373 (2003); https://doi.org/10.1016/S1386-1425(02)00337-2
19. K. Dai, H. Chen, T. Peng, D. Ke and H. Yi, *Chemosphere*, **69**, 1361 (2007); https://doi.org/10.1016/j.chemosphere.2007.05.021
20. Y. Liu, X. Chen, J. Li and C. Burda, *Chemosphere*, **61**, 11 (2005); https://doi.org/10.1016/j.chemosphere.2005.03.069
21. X.H. Liao, N.Y. Chen, S. Xu, S.B. Yang and J.J. Zhu, *J. Cryst. Growth*, **252**, 593 (2003); https://doi.org/10.1016/S0022-0248(03)01030-3
22. C. Wu, J.B. Shi, C.J. Chen, Y.C. Chen, Y.T. Lin, P.F. Wu and S.Y. Wei, *Mater. Lett.*, **62**, 1074 (2008); https://doi.org/10.1016/j.matlet.2007.07.046
23. R.S. Mane and C.D. Lokhande, *Mater. Chem. Phys.*, **65**, 1 (2000); https://doi.org/10.1016/S0254-0584(00)00217-0
24. M. Xu, H. Niu, J. Huang, J. Song, C. Mao, S. Zhang, C. Zhu and C. Chen, *Appl. Surf. Sci.*, **351**, 374 (2015); https://doi.org/10.1016/j.apsusc.2015.05.158
25. M. Wang, A.M. Anghel, B. Marsan, N.L. Cevey Ha, N. Pootrakulchote, S.M. Zakeeruddin and M. Gratzel, *J. Am. Chem. Soc.*, **131**, 15976 (2009); https://doi.org/10.1021/ja905970y
26. X. Fang, T. Song, R. Liu and B. Sun, *J. Phys. Chem. C*, **118**, 20238 (2014); https://doi.org/10.1021/jp506345a
27. Z. Yu, J. Meng, J. Xiao, Y. Li and Y. Li, *Int. J. Hydrogen Energy*, **39**, 15387 (2014); https://doi.org/10.1016/j.ijhydene.2014.07.165

28. S. Kong, Z. Jin, H. Liu and Y. Wang, *J. Phys. Chem. C*, **118**, 25355 (2014); https://doi.org/10.1021/jp508698q
29. D. Ayodhya, M. Venkatesham, A. Santoshi kumari, G.B. Reddy, D. Ramakrishna and G. Veerabhadram, *J. Exp. Nanosci.*, **11**, 418 (2016); https://doi.org/10.1080/17458080.2015.1070312
30. N. Soltani, E. Saion, M.Z. Hussein, M. Erfani, G. Bahmanrokh, A. Abedini, M. Navasery and P. Vaziri, *Int. J. Mol. Sci.*, **13**, 12242 (2012); https://doi.org/10.3390/ijms131012242
31. S. Chin, E. Park, M. Kim and J. Jurng, *Powder Technol.*, **201**, 171 (2010); https://doi.org/10.1016/j.powtec.2010.03.034
32. M. Asilturk, F. Sayilkan, S. Erdemoglu, M. Akarsu, H. Sayilkan, M. Erdemoglu and E. Arpac, *J. Hazard. Mater. B*, **129**, 164 (2006); https://doi.org/10.1016/j.jhazmat.2005.08.027
33. S.S. Arbuj, R.R. Hawaldar, U.P. Mulik, B.N. Wani, D.P. Amalnerkar and S.B. Waghmode, *Mater. Sci. Eng. B*, **168**, 90 (2010); https://doi.org/10.1016/j.mseb.2009.11.010
34. S. Dafare, P.S. Deshpande and R.S. Bhavsar, *Indian J. Chem. Technol.*, **20**, 406 (2013).
35. S. Bagwasi, B. Tian, J. Zhang and M. Nasir, *Chem. Eng. J.*, **217**, 108 (2013); https://doi.org/10.1016/j.cej.2012.11.080
36. Y. Gu, M. Xing and J. Zhang, *Appl. Surf. Sci.*, **319**, 8 (2014); https://doi.org/10.1016/j.apsusc.2014.04.182
37. D. Zhang, *Transition Met Chem.*, **35**, 933 (2010); https://doi.org/10.1007/s11243-010-9414-6
38. W. Fang, M. Xing and J. Zhang, *Appl. Catal. B*, **160–161**, 240 (2014); https://doi.org/10.1016/j.apcatb.2014.05.031
39. H.L. Wang, D.Y. Zhao and W.F. Jiang, *Desalination Water Treat.*, **51**, 2826 (2013); https://doi.org/10.1080/19443994.2012.750789
40. S. Mazumdar and A.J. Bhattacharyya, *RSC Adv.*, **5**, 34942 (2015); https://doi.org/10.1039/C5RA04733A
41. S.B. Kalia, D. Kumar, M. Sharma and J. Christopher, *J. Therm. Anal. Calorim.*, **120**, 1099 (2015); https://doi.org/10.1007/s10973-014-4342-x
42. E. Vijayakumar, A. Subramania, Z. Fei and P.J. Dyson, *RSC Adv.*, **5**, 52026 (2015); https://doi.org/10.1039/C5RA04944J
43. A. Pourahmad and Sh. Sohrabnezhad, *Mater. Lett.*, **65**, 205 (2011); https://doi.org/10.1016/j.matlet.2010.10.009
44. P. Scherrer and G. Nachar, *Math. Physik. Klasse*, **2**, 98 (1918).
45. X. Meng, J. Deng, J. Zhu, H. Bi, E. Kan and X. Wang, *Sci. Rep.*, **6**, 21717 (2016); https://doi.org/10.1038/srep21717
46. S.B. Sibokoza, M.J. Moloto, N. Moloto and P.N. Sibiya, *Chalcogenide Lett.*, **14**, 69 (2017).
47. S.S. Nath, D. Chakdar, G. Gope and D.K. Avasthi, *Nanotrends*, **2**, 20 (2007).
48. G. Yang, D. Gao, Z. Shi, Z. Zhang, J. Zhang, J. Zhang and D. Xue, *J. Phys. Chem. C*, **114**, 21989 (2010); https://doi.org/10.1021/jp106818p
49. R.W.Y. Man, A.R.C. Brown and M.O. Wolf, *Angew. Chem. Int. Ed. Engl.*, **51**, 11350 (2012); https://doi.org/10.1002/anie.201205057
50. J.R. Ferraro, Low Frequency Vibrations of Inorganic and Coordination Compounds, Plenum: New York (1971).
51. P. Borthakur and M.R. Das, *J. Colloid Interface Sci.*, **516**, 342 (2018); https://doi.org/10.1016/j.jcis.2018.01.050
52. C. Djebbari, E. Zouaoui, N. Ammouchi, C. Nakib, D. Zouied and K. Dob, *SN Appl. Sci.*, **3**, 255 (2021); https://doi.org/10.1007/s42452-021-04266-4
53. A.B. Lavand, M.N. Bhatu and Y.S. Malghe, *J. Mater. Res. Technol.*, **8**, 299 (2019); https://doi.org/10.1016/j.jmrt.2017.05.019
54. H. Ullah, E. Viglasova and M. Galambos, *Processes*, **9**, 263 (2021); https://doi.org/10.3390/pr9020263
55. T. Varadavenkatesan, E. Lyubchik, S. Pai, A. Pugazhendhi, R. Vinayagam and R. Selvaraj, *J. Photochem. Photobiol. B*, **199**, 111621 (2019); https://doi.org/10.1016/j.jphotobiol.2019.111621
56. S. Rajendrachari, P. Taslimi, A.C. Karaoglanli, O. Uzun, E. Alp and G.K. Jayaprakash, *Arab. J. Chem.*, **14**, 103180 (2021); https://doi.org/10.1016/j.arabjc.2021.103180